Characteristics of Electrically Driven Two-Dimensional Photonic Crystal Lasers

Hong-Gyu Park, Se-Heon Kim, Min-Kyo Seo, Young-Gu Ju, Sung-Bock Kim, and Yong-Hee Lee

***Abstract*—We demonstrate room-temperature low-threshold-current lasing action from electrically driven wavelength-scale high-quality photonic crystal lasers having large spontaneous emission factors by solving the theoretical and technical constraints laid upon by the additional requirement of the current injection. The ultrasmall cavity is electrically pulse pumped through a submicron-size semiconductor "wire" at the center of the mode with minimal degradation of the quality factor. In addition, to better utilize the low mobility of the hole, we employ a doping structure that is inverted from the conventional semiconductors. Rich lasing actions and their various characteristics are experimentally measured in the single-cell and three-cell photonic crystal cavities. Several relevant measurements are compared with three-dimensional finite-difference time-domain computations based on the actual fabricated structural parameters. The electrically driven photonic crystal laser, which is a small step toward a "practical" form of the single photon source, represents a meaningful achievement in the field of photonic crystal devices and photonic integrated circuits as well as of great interest to the quantum electrodynamics and quantum information communities.**

***Index Terms*—Current injection, finite-difference time-domain (FDTD), microcavity, photonic band gap, semiconductor laser, single photon source, spontaneous emission factor.**

I. Introduction

THE ULTIMATE smallest possible laser has long been a topic of central interest in laser and quantum optics [1]–[4] and recently gained renewed attention with the aid of the photonic crystal that enables strong photon confinement [5]–[9]. The photonic crystal cavity has a lot of merit as an efficient light emitter compared with the other types of microcavities: one can easily control distinct lasing properties such as wavelength, radiation direction, and near/far mode shapes by slight modification of lattice parameters [10]–[13]. Also, one can obtain a high quality (Q) factor and small modal volume simultaneously, which are the two main conditions of low-threshold lasers [14]–[18]. Since this small cavity supports only a few resonant modes, the ultimate thresholdless laser with a large spontaneous emission factor (β) near unity can be actualized [1], [10], [12], [19]. In addition, once the issue of coupling with a photonic crystal waveguide and/or a commercial tapered fiber is solved, photons extracted from the extremely small cavity can be efficiently utilized [20]. Finally, as a strong candidate of a single photon generator on chip, this ultrasmall cavity with a high Purcell factor has attracted many research groups [21].

Two-dimensional (2-D) photonic crystal InGaAsP slabs are widely used as a basic building block for various photonic devices [22]. When a photonic crystal cavity is formed, photons tend to be localized in the proximity of the photonic crystal resonator by the effects of photonic bandgap and total internal reflection [14]. So far, most of photonic crystal defect lasers have been operated by optical pumping [10]–[18], [23]–[26]. Electrically driven photonic band edge lasers were also reported with relatively large modal volume and threshold current [27]–[30]. However, only if one is able to activate the wavelength-scale laser electrically, can one talk about, with full confidence, standalone simple ultrasmall photon sources that operate with minimum power budget. Unfortunately, the electrical pumping of the wavelength-scale photonic crystal laser structure involves several critical issues that have to be answered. Therefore, the realization of viable structures has still remained the challenging and exciting issue of the community. As one of candidates of the electrically pumped structures, we have suggested the introduction of a small post at the center of the cavity [26], [31]. In that structure, it is possible to excite only those modes that have a node at the post position selectively because the other modes having a central antinode are suppressed by severe optical losses in the vertical direction. In addition, the post plays a role of a heat sink [26]. Thanks to this simple idea and delicate fabrication, we recently reported a novel electrically driven wavelength-scale high-Q photonic crystal laser structure [32].

We begin this paper by considering several design issues of our electrical pumping structure (Section II). Then we explain fabrication methods of a current blocking layer and a small central post in Section III. In the subsequent sessions, various characteristics of the photonic crystal lasers are analyzed. Throughout the paper, several relevant experimental results are compared with three-dimensional (3-D) finite-difference time-domain (FDTD) computations which are performed by the structure obtained from the actually fabricated sample.

II. Design of Electrical Contact

Several photonic crystal structures suitable for electrical pumping have been suggested [33]–[35]. Among them, photonic band edge lasers were realized first, thanks to their relatively large active volume and the simple current confinement [27]–[30]. On the other hand, the ultrasmall photonic crystal defect laser was recently demonstrated after solving

Manuscript received March 17, 2005; revised April 24, 2005. This work was supported in part by the National Research and Development Project for Nanoscience and Technology.

H.-G. Park is with the Department of Chemistry and Chemical Biology, Harvard University, Cambridge, MA 02138 USA (e-mail: ppakkong9@gmail.com).

S.-H. Kim, M.-K. Seo, and Y.-H. Lee are with the Department of Physics, Korea Advanced Institute of Science and Technology, Daejeon 305-701, Korea (e-mail: seheon@kaist.ac.kr; physics0510@kaist.ac.kr; yhlee@kaist.ac.kr).

Y.-G. Ju and S.-B. Kim are with the Telecommunication Basic Research Laboratory, Electronics and Telecommunications Research Institute, Daejeon 305–701, Korea (e-mail: ygju@knu.ac.kr; sbk@etri.re.kr).

Digital Object Identifier 10.1109/JQE.2005.852800

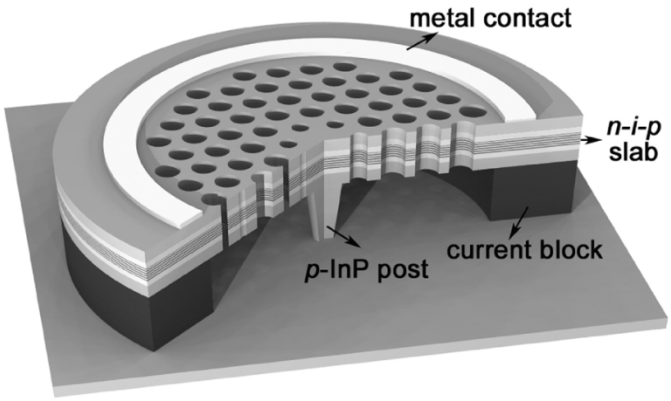

(a)

Material	Thickness	Doping (cm^{-3})	Remark
n-InP	0.1 μm	~ $1.1x10^{18}$	Capping layer, removed
n-1.24Q InGaAsP	600 Å	~ $2.7x10^{19}$	Delta doping
i-1.24Q InGaAsP	200 Å	Undoped	
1.30Q (-0.5%) InGaAsP	115 Å	Barrier	6 pairs, λc = 1.55 μm
1.65Q (+0.8%) InGaAsP	70 Å	Well	
1.30Q (-0.5%) InGaAsP	115 Å	Barrier	
i-1.24Q InGaAsP	200 Å	Undoped	
p-1.24Q InGaAsP	600 Å	~ $3x10^{18}$	
p-InP	1.0 μm	~ $1.5x10^{18}$	Sacrificial layer (post)
p-InGaAs	0.1 μm	~ $5x10^{18}$	Etch-stop layer
p-Buffer InP	0.3 μm	~ $1x10^{18}$	
p-InP substrate			

(b)

Fig. 1. (a) Schematic diagram of the free-standing slab structure for current injection. (b) Designed wafer structure.

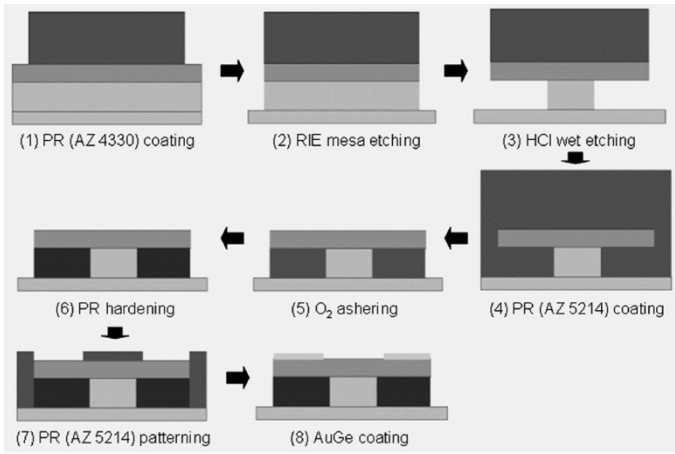

(a)

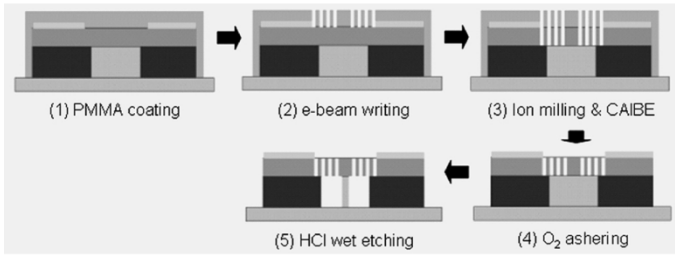

(b)

Fig. 2. Schematic diagrams of fabrication processes of (a) mesa structure and (b) photonic crystal patterns.

the issue of current injection into the small cavity [32]. Both electrical and optical confinements inside that cavity should be effectively actualized. One possible way to inject current into the slab with a periodic pattern could be found in the microdisk structure [3], [36]. Small posts are positioned below and above the microdisk and act as the current channel into an active material embedded inside the cavity. In our photonic crystal structure, we place only one post under the slab as an electrical contact and substitute the other one with a large metal contact around the cavity as in conventional semiconductor devices [37]–[39]. Because the size of the photonic crystal cavity is much smaller than that of the microdisk, a two-post-structure cannot guarantee the mechanical stability. The topmost layer of the semiconductor slab is heavily n-doped over $10^{18}/\mathrm{cm}^3$. In particular, the formation of the n-i-p heterojunction slab increases overall injection efficiency of the carriers into the cavity since the mobility of electrons is larger than that of holes [38]. In this configuration, holes that are supplied through the post do not diffuse far from the center and electrons and holes recombine mostly near the central post. Experimentally, the post formation in the ultrasmall cavity is nontrivial. We decided to place the post at the center of the cavity and to select the optical mode with a central intensity node. For these modes, the introduction of a small central post does not degrade the Q factor of the mode significantly [12], [26]. On the other hand, those modes with central anti-nodes are discarded because they undergo unavoidable optical losses through the central post. A schematic diagram of our structure is shown in Fig. 1(a).

Characteristics of the resonant mode having a central node have been already studied in theory and experiment [12]. In particular, the monopole and hexapole modes attract our attention because of the merits of the nondegeneracy, high Q factors and small modal volumes. These modes can be found in a modified single-cell cavity [10], [12]. We are particularly interested in the monopole mode because the resonance of the mode is spectrally well-separated from the other resonant modes.

III. Fabrication

Fig. 1(b) shows our bare wafer structure. Six intrinsic and strain-compensated InGaAsP quantum wells (QWs) and highly doped n- and p- layers are employed. In particular, note that the delta doping layer in the top layer of the thin slab is contained.

In the case of the microdisk, the slab is mechanically supported by the pedestal structure [3], [36]. However, for the photonic crystal cavity, the central post is much smaller and weaker and therefore mechanically unstable. We need to insert dielectric material under the slab to support the relatively large slab structure. In the structure shown in Fig. 1(a), the dielectric material consisting of photoresist (PR) is acting also as a current blocking layer [32]. Several complicated fabrication processes are required to produce this structure [Fig. 2(a)]. First, mesas with a diameter of $\sim 50\ \mu$m are formed for electrical isolation by dry etching processes. Thick PR with thickness of $\sim 3\ \mu$m is used as a mask for CH_4/H_2 reactive ion etching (RIE) plasma etching. Then, a $\sim 13 \times 13$-$\mu\mathrm{m}^2$-large p-InP layer post remains

at the center and the other sacrificial InP region is etched by diluted HCl solution $(\mathrm{HCl{:}H_2O} = 2:1)$ at room temperature for ~ 7 min. If the thick PR mask is removed before the wet etching process, some parts of undercut slab would stick to the bottom of wafer due to the van der Waals force between two surfaces. But, in our step, the thick PR prevents the collapse of the pedestal structure. The etched region is filled with a dielectric material (another PR) for mechanical stability by spin coating. Now, all surfaces of the mesa including the etched region are coated by the PR. Subsequent O_2 ashering removes the entire exposed PR except that is hidden under the slab. If thin Si_xN_y or SiO_2 layers had been coated below the first PR mask, all remnants of the PRs after the ashering process could be peel off by immersing the wafer in buffered oxide etch (BOE) solution. The blocking layer by PR is hardened at temperature over 250 °C. After the ring-shaped AuGe metal contact is formed, fabrication of the first post surrounded by the current blocking layer is finished.

We have also tried several other methods in order to construct the current blocking layer besides the above trial. First, we tried the selective ion implantation scheme where only a specific region has a high electrical resistance and the desired current path can be designed [37], [39]. If heavy ions such as Fe and Cl are injected into the p-InP layer below the active layer, current is expected to flow only through the nonattacked region. Although this method looks easy and simple, the exact location and range of the bombing region were difficult because the semiconductor slab is very thin. Actually, in our fabricated samples, the current flow was not easily confined and/or QWs embedded in the slab were damaged by the heavy ions. In the other trial, we tested selective oxidation techniques [39] using a different wafer structure: instead of the sacrificial InP layer below the slab, an Al-containing layer is placed and oxidized to a dielectric layer with low refractive index. If we use InAlAs material, the oxidation time gets very slow and QWs are damaged by the high temperature of the oxidation process [39]. To avoid this damage, we added a fusion technique by which a GaAlAs layer is put under the slab [23], [24], [39]. Through a standard oxidation procedure, effective current confinement structure is expected [33]. However, this method also has serious problems in the subsequent processes and we failed to obtain the unoxidized small post of diameter ~ 1 μm because of the delicate second oxidation process. Furthermore, the unoxidized region is not generally formed at the center of the resonator.

In the following steps shown in Fig. 2(b), photonic crystal patterns and a small central post are fabricated. The lattice parameters are designed such that the monopole mode is located in the middle of photonic band gap. Fig. 3 shows a scanning electron miscroscope (SEM) picture of the fabricated photonic crystal structure whose lattice parameters are as follows: $a = \sim 510$ nm, $r_I = 0.28\ a$, $r_{II} = 0.35\ a$, $r_{III} = 0.385\ a$, $r_{IV} = 0.4\ a$, $r_V = 0.41\ a$, where a is the lattice constant, r_i is radius of the air hole in the ith region, respectively. The radii of the air holes in the ith region are all same. Note that the radii of the air holes are continuously changed and the smallest near the cavity. The main purpose of this specifically modified structure is to place the post at the center below the cavity during the etching process. The post is formed by HCl etching ($\mathrm{HCl{:}H_2O} = 2{:}1$) at low temperature near 10°C. The lateral etching rate tends to depend on the size of air holes through which diluted HCl is supplied, and we achieve better control of the position and size of the central post by introducing chirped air holes shown in Fig. 3. These chirped air holes turn out to increase the Q factor and the modal volume of the cavity slightly. This fact is confirmed by 3-D FDTD calculations for an ideal structure with circular air holes and without a post. In our fabrication, the wet etching time is actually ~6 min which is sensitive and changeable by the previous dry etching time, cleaning of the wafer and surrounding air temperature. Fig. 4 shows an SEM picture of a fabricated post where the slab is intentionally broken to expose the post. In Fig. 5(a) and (b), we also see the clear formation of the central post. Here we delicately cut a small portion including a half of the cavity by focused ion beam (FIB) etching. During this etching process, the end facet of the slab is affected by the heavy ions [Fig. 5(a)] and InP remnants are sputtered around the post and the slab edge [Fig. 5(b)]. So the post looks thick compared to its real shape.

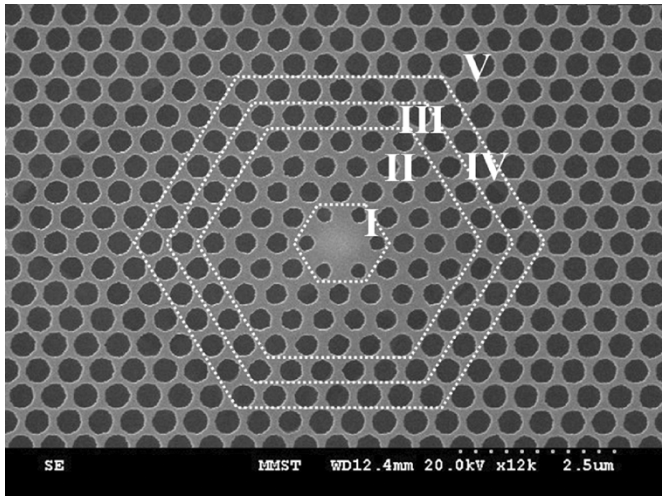

Fig. 3. SEM picture (top view) of a fabricated photonic crystal structure.

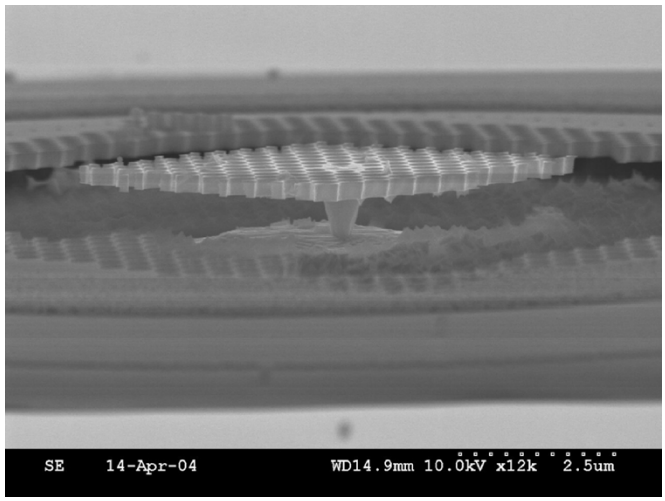

Fig. 4. Cross-sectional SEM image. Dusts around the post are remnants of the PR produced in the intentional breaking process.

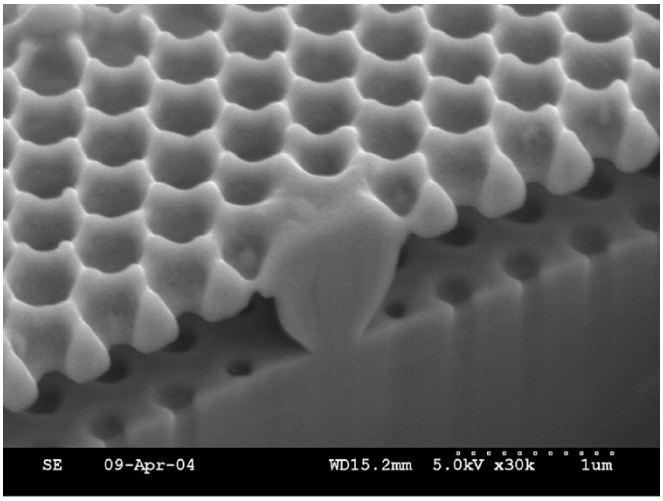

(a)

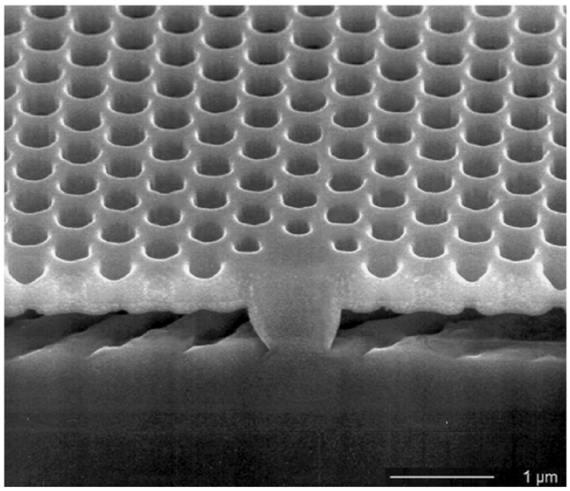

(b)

Fig. 5. (a)–(b) SEM pictures of the post structures. The region around the cavity is cut by FIB machine.

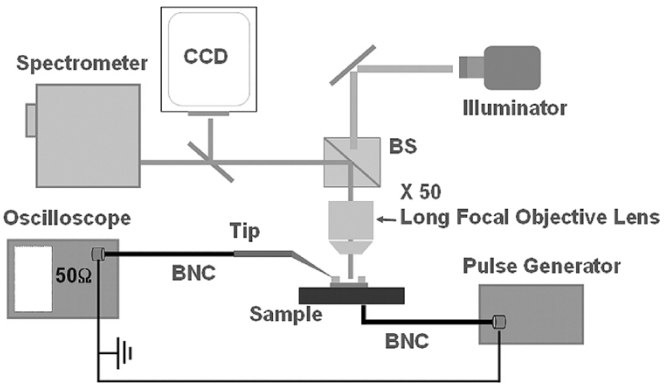

Fig. 6. Schematic diagram of the experimental setup for current injection.

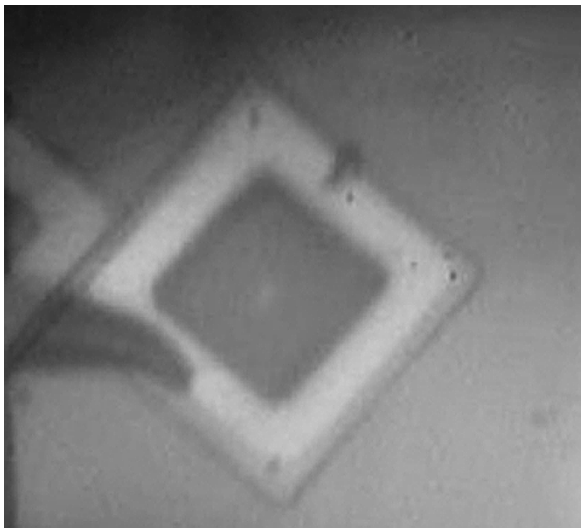

Fig. 7. Mesa structure and a current-supplying metal tip captured by an IR camera.

IV. Single-Cell Lasers

A. Experimental Setup

The output photons of the electrically pumped single-cell photonic crystal laser are collected through a 50× long-focal microscope objective lens (numerical aperture of 0.42) and fed into a spectrometer as shown in Fig. 6. In an image captured by an infrared (IR) camera (Fig. 7), a current-supplying metal tip touches the top-metal-contact of the laser structure. To minimize electrical noises, the fabricated sample is attached on a very small metal plate by silver paste connected by a bayonet-type connection (BNC) cable. By measuring voltage V from the oscilloscope, peak current I was obtained.

For comparison, electrical and optical properties of the post structure without photonic crystal pattern are also measured. The electroluminescence (EL) spectrum with a center peak of 1.5-μm wavelength is observed in Fig. 8(a). In this case, it is operated by input peak-to-peak voltage of 2 V at room temperature. Fig. 8(b), directly captured from the oscilloscope, shows good electrical characteristics of the fabricated pedestal structure. In this current–voltage $(I$–$V)$ curve, we obtain turn-on voltage of $\sim$0.5 V and small electrical resistance of $\sim$ 60 Ω, respectively.

B. Lasing Properties

From the cavity of Fig. 3, room-temperature single-mode lasing action is observed at wavelength of 1519.7 nm, as shown in Fig. 9(a). Due to the large thermal resistance (346 K/mW) of the small post structure [38], [40], the laser is operated in a pulsed mode with duty cycle of $\sim$0.24%. The pulsewidth and period are $\sim$6 ns and 2.5 μs, respectively. Above threshold, the spectral linewidth of this nondegenerate lasing mode becomes spectrometer-limited at $\sim$0.55 nm. In order to identify the lasing mode, the mode profile and polarization direction are measured. In Fig. 9(b), the lasing mode with a central intensity minimum and a donut-shaped intensity distribution is captured by an IR camera. Here the white bar represents a 2-μm ruler and the white hexagon means region (II)/(III) interface in Fig. 3. Also, no preferred polarization direction is observed from the top [Fig. 9(c)]. This is one of the unique characteristics expected from the monopole mode [10], [12]. The inset of Fig. 9 shows a below-threshold spectrum measured at 200 μA. In the coarse resolution regime of the spectrometer, we can find the other nonlasing resonant mode near 1491 nm as well. This

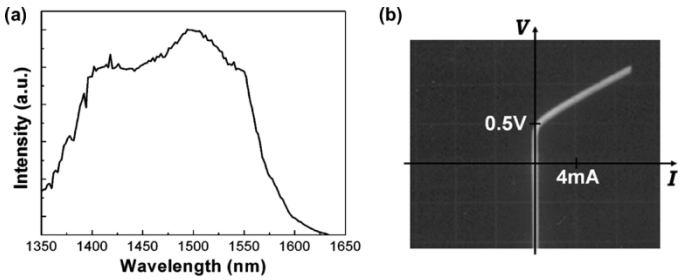

Fig. 8. (a) EL spectrum measured from a fabricated mesa structure. (b) I–V curve of the mesa structure operated by input peak-to-peak voltage of 2 V.

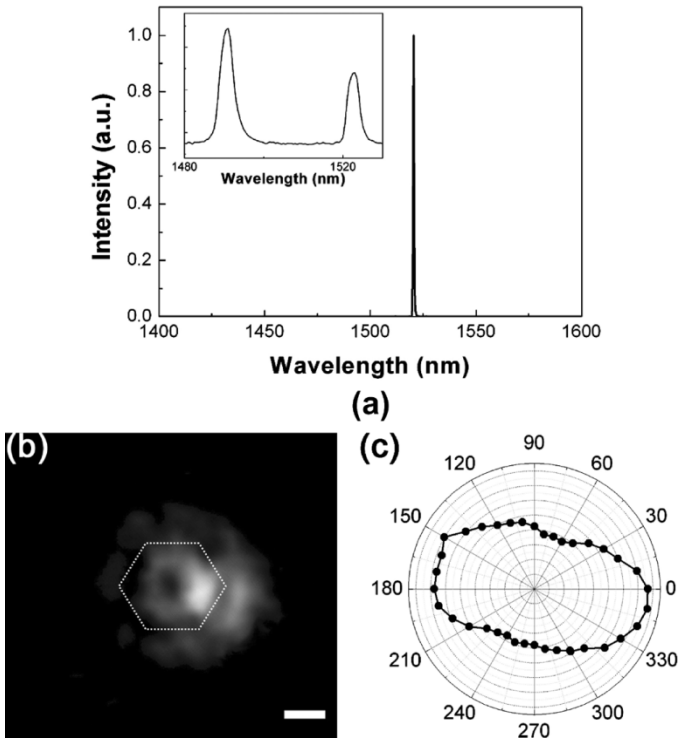

Fig. 9. (a) Lasing spectrum measured at 700 μA. In inset, the other nonlasing resonant mode is found when the injected current is 200 μA and the slit-width of the spectrometer becomes >5 times broader. (b) Near-field image of the monopole mode captured by an IR camera. (c) Measured polarization state of the monopole-mode laser. The direction is the same as that of the hexagon in (b).

mode (the second quadrupole mode) did not lase because of the low Q factor of <700 [12].

Experimental data are compared with the results computed by the 3-D FDTD method. To remove any unnecessary argument about the validity and accuracy of this comparison, we use the numerical data derived directly from the SEM image as the structural input data file of our FDTD computation [32]. In this case, all the imperfections introduced during the fabrication processes are included faithfully. We can divide inside and outside the air holes according to the colors shown in SEM image and separately add the pedestal structure in vertical direction. Fig. 10 shows the actual transformation process from the SEM image to the structure for our calculation. The resonant frequency and mode shape (Fig. 11) of the monopole mode agreed well with the experimental results. In particular, Fig. 11(b)–(e), vertical components of the Poynting vector calculated at various

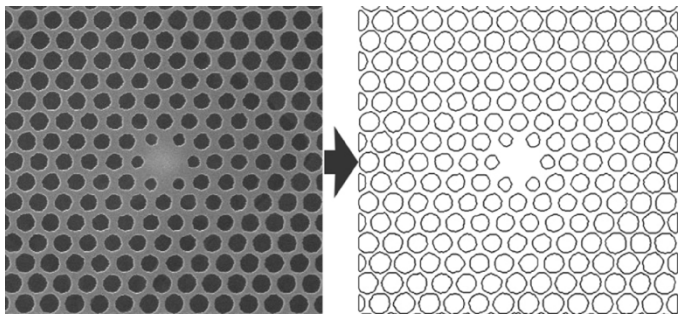

Fig. 10. Transformation from a SEM picture to the structure employed in the calculation domain.

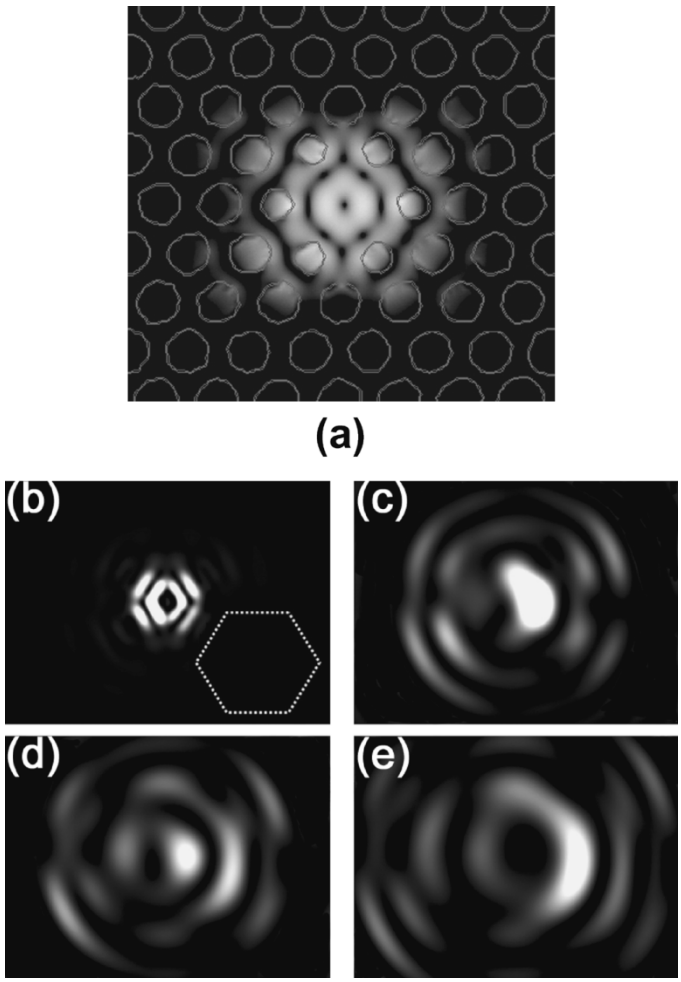

Fig. 11. (a) Electric field intensity profile at the center of the slab (log scale). For comparison, vertical components of Poynting vector are computed at various vertical positions: (b) $z = a$; (c) $z = 4\ a$; (d) $z = 6\ a$; and (e) $z = 8\ a$, where the origin is the center of the slab and a is lattice constant (linear scale). The white hexagon with the same size as that of Fig. 9(b) is shown as a scale bar. Maximum intensity values of (b)–(d) are 100, 3, and 1.5 times larger than that of (e), respectively.

vertical positions above the slab are obtained to be directly compared with the experimental picture of Fig. 9(b). The intensity profile of the monopole mode, which is confined in the slab, is shown in Fig. 11(a) as a reference.

The measured Q factor of a cold cavity for the monopole mode, as estimated from the spectral linewidth associated with a transparent current of $\sim$ 225 μA, is $\sim$>2500. The transparent

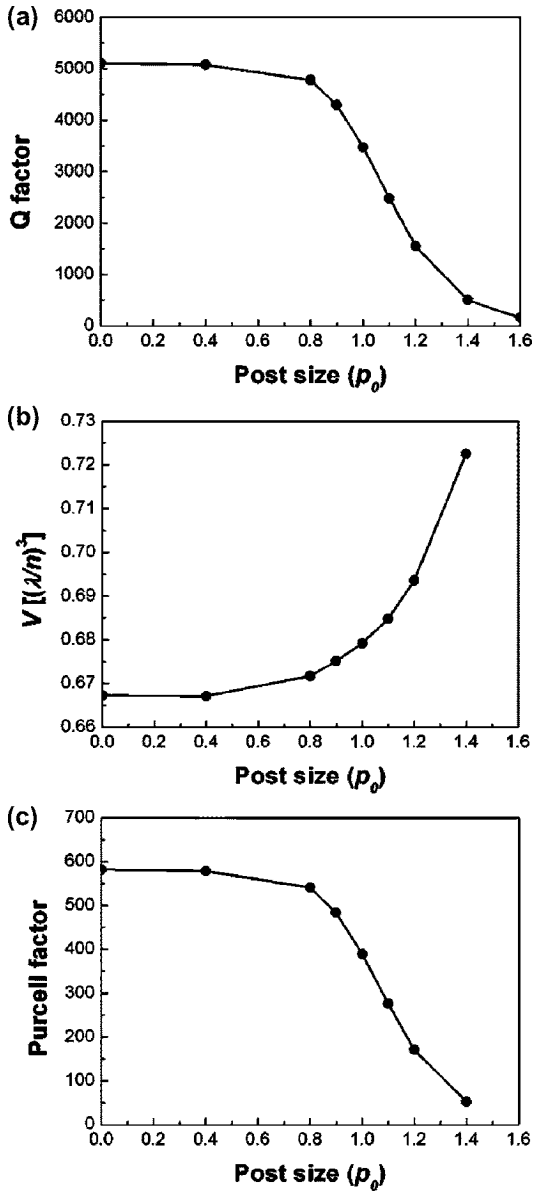

Fig. 12. (a) Q factor, (b) modal volume, and (c) Purcell factor computed by the actual structural data of Fig. 3.

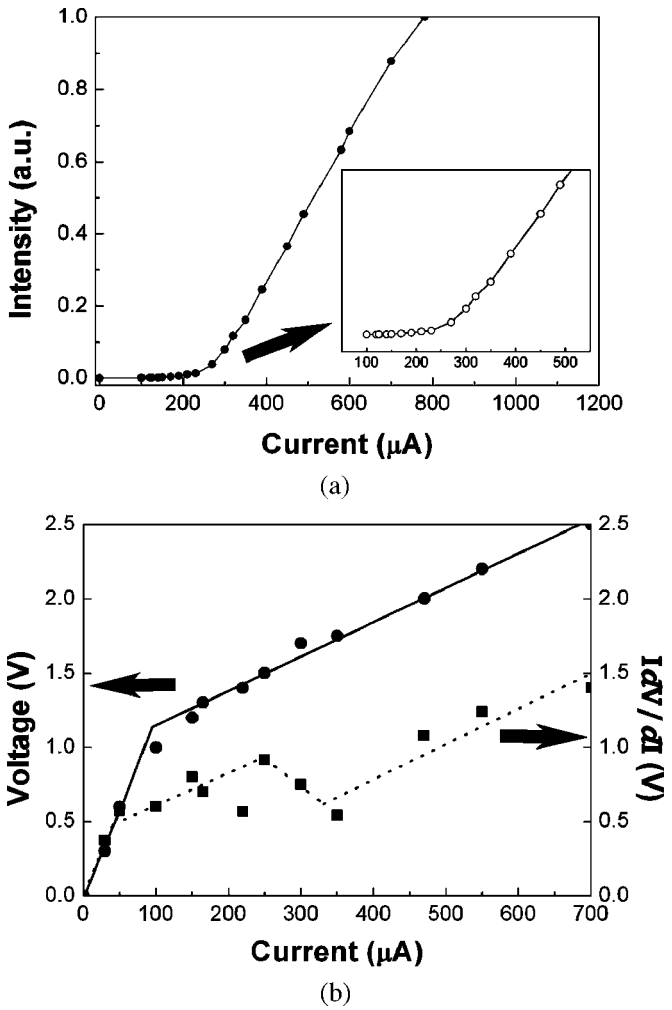

Fig. 13. (a) L–I curve of the monopole-mode laser. Soft turn-on near the threshold is observed (inset). (b) Typical electrical characteristics of the laser.

current is determined by solving the rate equation that will be discussed later [10], [18]. To compare this Q factor with computed one, the size of the diamond-like post is estimated from the SEM image of Fig. 3. Let p_0 be the estimated post size ($0.64a \times 0.51a$ in diagonal directions) and then Q factors are calculated as a function of multiples of p_0. In Fig. 12(a), the Q factor at p_0 (3480) compares well with the experimental value. In addition, the Q factor degrades rapidly when the post size becomes larger than p_0. On the other hand, electrical and thermal resistances will be increased more with the smaller post size [38], [40]. Thus, the post size should be optimized to obtain a stable lasing operation with better optical, electrical and thermal properties. Fig. 12(b) and (c) shows the computed modal volume and Purcell factor of the monopole mode as a function of the post size, respectively. At p_0, we obtain the small modal volume of 0.68 $(\lambda/n)^3$ and the large Purcell factor of 389, where n is a refractive index of the slab. Due to the large Purcell factor of the monopole mode, one could observe cavity quantum electrodynamics (CQED) effects in this electrically driven small and high-Q cavity with the unique mode shape [4], [41].

The peak output intensity is shown as a function of the peak input current in Fig. 13(a). In this L–I curve, we can determine the threshold value of $\sim$ 260 μA. This low threshold compares favorably with those estimated from the optical pumping experiment [12]. In Fig. 13(b), electrical characteristics, I–V and $I\ dV/dI$–I, curves of this single-cell photonic crystal laser are measured. From these curves, relatively high electrical resistance of $\sim$ 2.2 $k\Omega$ is obtained, which is mainly attributed to the submicron size of the p-InP post. Noticeable current leakage is also observed due to the nonradiative recombination at the air/semiconductor interfaces of air holes and the mesa edge [38]. If this non-negligible leakage is reduced, the threshold current could be smaller. Additionally, note that there is a clear kink near the threshold in the $I\ dV/dI$–I curve [42].

For comparison purposes, an electrically driven monopole-mode laser is also optically pulse-pumped. Under similar pulse conditions, we confirmed the monopole mode lasing at almost an identical resonant frequency.

TABLE I
EMPLOYED PARAMETERS IN THE RATE EQUATION

Parameters	Values
Internal efficiency, η_i	0.25
Confinement factor, Γ	0.175
Surface recombination velocity, v_s	1.2×10^4 cm s^{-1}
Bimolecular radiative coefficient, B	1.6×10^{-10} cm^3 s^{-1}
Auger coefficient, C	5.0×10^{-29} cm^6 s^{-1}
Transparent carrier density, N_{tr}	1.5×10^{18} cm^{-3}
Active volume, V_a	1.72×10^{-13} cm^3
Active surface area, A_a	1.47×10^{-8} cm^2
Quality factor, Q	2500
Lasing wavelength, λ	1519.7 nm
Gain coefficient, G_0	1500 cm^{-1}
Equivalent refractive index, n_{eq}	2.9067

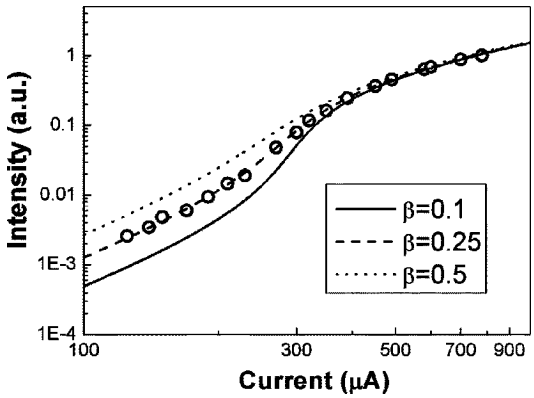

Fig. 14. Comparison of the measured *L–I* curves (dots) with those obtained from the rate equations (lines) for the monopole mode.

C. Spontaneous Emission Factor

As shown in inset of Fig. 13(a), a soft turn-on near the threshold implies a large β value [12]. To quantify the β value, we employ the laser rate equations where various parameters are required. Typical material parameters of InGaAsP QWs are used [12], [36], [43]. In addition, several important parameters are experimentally determined to reduce the ambiguity of the estimation. Actually, the size of the light emitting region, one of the critical parameters, is obtained directly from the EL profile under the transparent condition [32]. All parameters used for the computation are summarized in Table I. The spectrally integrated experimental data points (dots) are plotted together with those obtained from the rate equations (lines), for the monopole mode, in the log-log graph of Fig. 14. The β value of $\sim$0.25 seems to fit the experimental value best. This is the record-high β value among those reported from the semiconductor nanolasers [12], [36], [43], [44]. The large β value is ascribed to the effective carrier localization by electrical pumping together with the nondegeneracy and the small mode volume [1], [12], [45].

The reliability of this β value estimation is examined as we vary fitting parameters. First, the dependence of β on the Auger coefficient (C) is considered as a function of the wafer temperature. The value of C could increase $3 \sim 4$ times when the wafer temperature increases up to $\sim$420 K from room temperature [46]. This is the worst possible scenario imaginable from a freestanding cavity by a pulsed operation with larger duty cycle of 4% [47]. Even under this harsh condition, β changes only slightly from 0.25 to 0.23. Therefore, we argue that β depends only very modestly on the Auger recombination. Next, the β value is computed as we change the cavity Q value and found $(Q, \beta) = (2000, 0.2)$ $(2100, 0.215)$, $(2200, 0.23)$, $(2300, 0.25)$, $(2500, 0.25)$, $(2700, 0.29)$, $(3000, 0.33)$, and $(3480, 0.38)$. Here, the computed Q value of 3480 by the 3-D FDTD method can be considered as an upper bound. Actually, we obtain a Q factor larger than 2500 from a measured linewidth in the estimated range of transparency. Therefore, the actual β value can be larger than 0.25. In addition, the spatial distribution of carriers by diffusion is indirectly considered in our simple rate equations. Slight variations of the parameters other than the surface recombination are tolerable in the fitting of β. Since the critical parameters including the surface recombination are obtained from experimental data, our estimation is believed to be not very far from the real value.

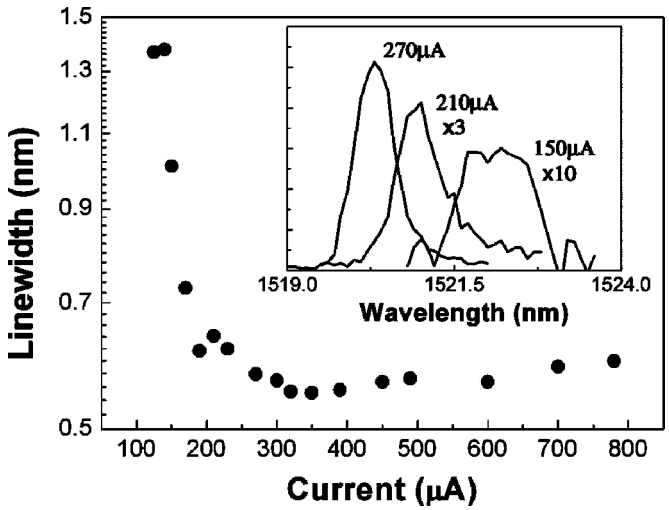

Fig. 15. Linewidth of the monopole mode is measured as a function of the injected current. In inset, three selected spectra are shown.

The semiconductor microlaser with a very large β value can have a linewidth wider than those of typical lasers [48]. Also, it was reported that lasing linewidth remains nearly constant as the pumping level increases if the β value of a laser mode is above 0.05 [49]. In order to confirm this property in our laser, the linewidth of the monopole mode is measured as a function of injection current as shown in Fig. 15. Note that linewidth drastically changes near the threshold ($\sim$ 260 μA) and approached the resolution-limit of the spectrometer $\sim$ 0.55 nm. Since the measured linewidth is immediately saturated above the threshold, we cannot insist that this changing behavior of the linewidth has the same origin as that of [49]. However, from this experiment, we can clearly identify the position of the lasing threshold again.

Properties of another monopole-mode laser fabricated with different lattice parameters are measured and shown in Fig. 16. In this laser structure, the radius of the nearest neighbor air holes

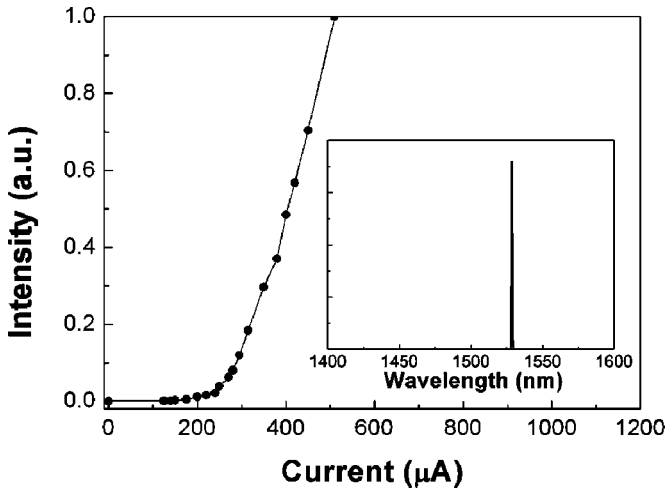

Fig. 16. L–I curve of another monopole-mode laser with different lattice parameters. In inset, the lasing spectrum taken at 510 μA is shown. The intensity of the lasing peak is $>$30 dB larger than that of the background.

around the cavity is slightly reduced to $0.25\,a$ from $0.28\,a$ while the other parameters are unchanged. Compared to the previous monopole-mode laser, the threshold current of this laser is almost identical and the β value (~ 0.15) is somewhat smaller.

V. Three-Cell Lasers

The three-cell photonic crystal cavity allows a central post somewhat larger than that of the single-cell cavity, and the fabrication of a larger post by the wet etching process becomes less delicate. In fact, we fabricated a three-cell laser cavity first to observe lasing action [50]. Using the same wafer structure of Fig. 1(b), various photonic crystal cavities are fabricated and tried. We begin measurement with the three-cell cavity of Fig. 17(a) where only the nearest air holes around the cavity are modified. At the center of the cavity, the central post (white shadow region) is shown. Structural parameters are as follows: lattice constant a is $\sim$455 nm and the radii of the each of the air holes are $0.37\ a$ and $0.4\ a$, respectively. Experimental characteristics of this structure are shown in Fig. 17(b). In the inset of this figure, several nonlasing resonance peaks are observed owing to its large cavity size. Also, the peak output intensity is plotted as a function of the peak input current. Here the threshold current is 600 μA, which is somewhat larger than that of the single-cell laser. Since the wider area around the cavity needs to be pumped, the threshold value increases naturally. The lasing mode is linearly polarized.

Interestingly, even from the three-cell cavity with an off-centered post, lasing action is observed as shown in Fig. 18. The threshold current is $\sim$ 650 μA, and the off-centered post leads to a linear polarization state whose direction is determined by the position of the post.

The effect of the size of the central post is also studied. From Fig. 19(a)–(d), etching times are increased and post sizes are reduced gradually. The etching time of each figure differs by several tens of seconds. We cannot obtain lasing action in the case of (a) due to the serious optical loss through a large central post. On the other hand, as the size decreases [(b) and (c)], a few nonlasing additional resonant modes begin to show up in the gain spectrum. Finally, lasing action is observed in the optimized post size of (d). All measurements are performed under the same conditions.

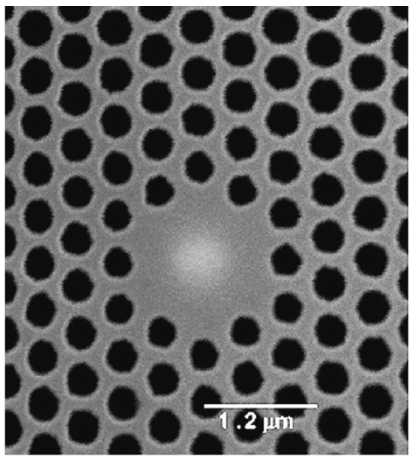

(a)

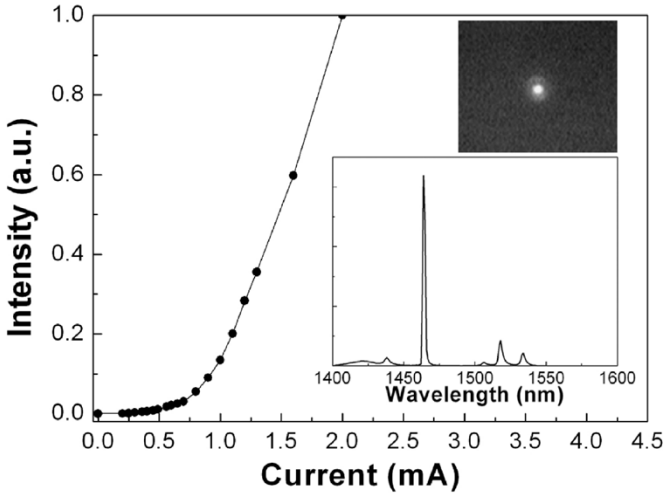

(b)

Fig. 17. (a) Top view of a three-cell laser cavity. (b) Measured L–I curve, above-threshold spectrum and mode profile (inset).

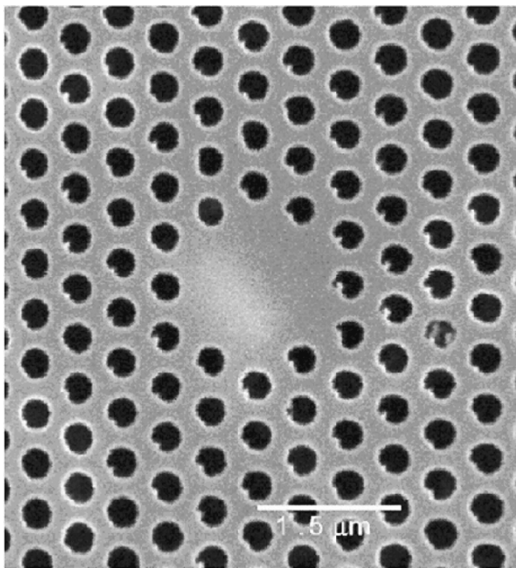

Fig. 18. SEM image of the three-cell cavity with an off-centered post.

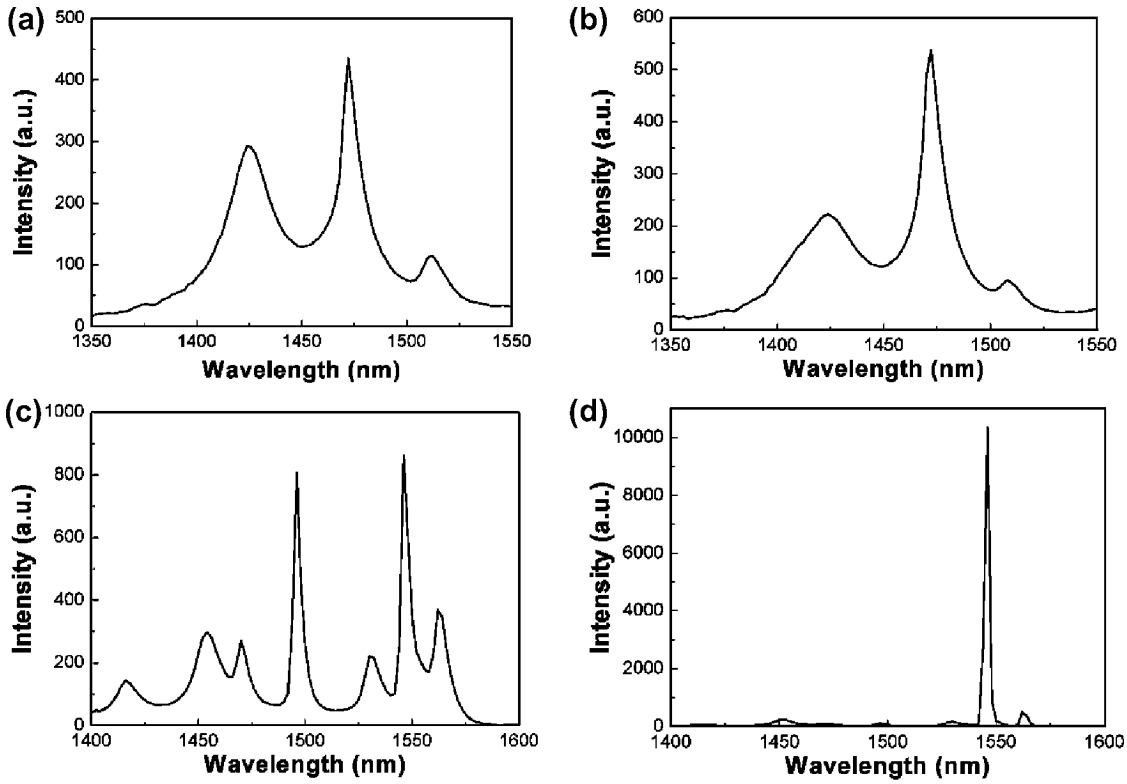

Fig. 19. (a)–(d) EL spectra obtained by various wet etching times in a three-cell cavity. The etching time of (a) is ∼6 min and each one of (a)–(d) differs by several tens of seconds.

VI. Summary

We successfully fabricated an electrically driven, low-threshold, single-cell photonic bandgap laser at room temperature. This laser shows extremely small mode volume $(5.87 \times 10^{-2}\ \mu\text{m}^3)$, low threshold current $(\sim 260\ \mu\text{A})$, and large spontaneous emission factor (~ 0.25). By measuring its lasing spectrum, near-field image and polarization state, we confirm that our lasing mode is the high-Q, nondegenerate monopole mode with central node. Additionally, we investigated the other photonic crystal laser structures and their characteristics.

The threshold of our laser is slightly larger than our expectation. From the rate equations, the single-cell photonic crystal laser with very high-Q factor and small modal volume can have ultralow threshold less than 100 μA, as reported in microdisk lasers [43]. The main origin of this large threshold is the nonradiative recombination at surfaces of lots of air holes. To reduce this effect, some passivation process can be added in the fabrication [38] or quantum dots (QDs) can be employed as an active material [25]. In particular, injection of a single QD into the small cavity will be a meaningful step to observe CQED effects by a large Purcell factor and to realize the thresholdless laser.

Acknowledgment

The authors would like to thank Prof. Koyama of Tokyo Institute of Technology for offering SEM pictures of samples processed by the FIB machine, and Prof. J. Shim, Hanyang University, for helpful discussions.

References

[1] H. Yokoyama, "Physics and device applications of optical microcavities," *Science*, vol. 256, pp. 66–70, 1992.
[2] G. Björk and Y. Yamamoto, "Analysis of semiconductor microcavity lasers using rate equations," *IEEE J. Quantum Electron.*, vol. 27, no. 12, pp. 2386–2396, Dec. 1991.
[3] T. Baba, "Photonic crystals and microdisk cavities based on GaInAsP-InP system," *IEEE J. Sel. Topics Quantum Electron.*, vol. 3, no. 3, pp. 808–830, Jun. 1997.
[4] K. J. Vahala, "Optical microcavities," *Nature*, vol. 424, pp. 839–846, 2003.
[5] E. Yablonovitch, "Inhibited spontaneous emission in solid-state physics and electronics," *Phys. Rev. Lett.*, vol. 58, pp. 2059–2062, 1987.
[6] S. John, "Strong localization of photons in certain disordered dielectric superlattices," *Phys. Rev. Lett.*, vol. 58, pp. 2486–2489, 1987.
[7] J. D. Joannopoulos, R. D. Meade, and J. Winn, *Photonic Crystals: Molding the Flow of Light*. Princeton, NJ: Princeton Univ. Press, 1995.
[8] J. D. Joannopoulos, P. R. Villeneuve, and S. Fan, "Photonic crystals: putting a new twist on light," *Nature*, vol. 386, pp. 143–148, 1997.
[9] T. F. Krauss and R. M. De La Rue, "Photonic crystals in the optical regime-past, present and future," *Prog. Quantum Electron.*, vol. 23, pp. 51–96, 1999.
[10] H. G. Park, J. K. Hwang, J. Huh, H. Y. Ryu, Y. H. Lee, and J. S. Kim, "Nondegenerate monopole-mode two-dimensional photonic bandgap laser," *Appl. Phys. Lett.*, vol. 79, pp. 3032–3034, 2001.
[11] H. Y. Ryu, S. H. Kim, H. G. Park, J. K. Hwang, Y. H. Lee, and J. S. Kim, "Square-lattice photonic bandgap single-cell laser operating in the lowest-order whispering gallery mode," *Appl. Phys. Lett.*, vol. 80, pp. 3883–3885, 2002.
[12] H.-G. Park, J.-K. Hwang, J. Huh, H.-Y. Ryu, S.-H. Kim, J.-S. Kim, and Y.-H. Lee, "Characteristics of modified single-defect two-dimensional photonic crystal lasers," *IEEE J. Quantum Electron.*, vol. 38, no. 10, pp. 1353–1365, Oct. 2002.
[13] S.-H. Kim, H.-Y. Ryu, H.-G. Park, G.-H. Kim, Y.-S. Choi, Y.-H. Lee, and J.-S. Kim, "Two-dimensional photonic crystal hexagonal waveguide ring laser," *Appl. Phys. Lett.*, vol. 81, pp. 2499–2501, 2002.

[14] O. Painter, R. K. Lee, A. Scherer, A. Yariv, J. D. O'Brien, P. D. Dapkus, and I. Kim, "Two-dimensional photonic bandgap defect mode laser," *Science*, vol. 284, pp. 1819–1821, 1999.
[15] O. Painter, J. Vuckovic, and A. Scherer, "Defect modes of a two-dimensional photonic crystal in an optically thin dielectric slab," *J. Opt. Soc. Amer. B*, vol. 16, pp. 275–285, 1999.
[16] O. J. Painter, A. Husain, A. Scherer, J. D. O'Brien, I. Kim, and P. D. Dapkus, "Room temperature photonic crystal defect lasers at near-infrared wavelengths in InGaAsP," *J. Lightw. Technol.*, vol. 17, no. 11, pp. 2082–2088, Nov. 1999.
[17] M. Loncar, T. Yoshie, A. Scherer, P. Gogna, and Y. Qiu, "Low threshold photonic crystal laser," *Appl. Phys. Lett.*, vol. 81, pp. 2680–2682, 2002.
[18] K. Srinivasan, P. E. Barclay, O. Painter, J. Chen, A. Y. Cho, and C. Gmachl, "Experimental demonstration of a high quality factor photonic crystal microcavity," *Appl. Phys. Lett.*, vol. 83, pp. 1915–1917, 2003.
[19] R. De La Rue and C. Smith, "On the threshold of success," *Nature*, vol. 408, pp. 653–656, 2000.
[20] K. Srinivasan, P. E. Barclay, M. Borselli, and O. Painter, "Optical-fiber-based measurement of an ultrasmall high Q photonic crystal microcavity," *Phys. Rev. B*, vol. 70, p. 081306, 2004.
[21] J. M. Gerard and B. Gayral, "Toward high-efficiency quantum-dot single-photon sources," *Proc. SPIE Int. Soc. Opt. Eng.*, vol. 5361, pp. 88–95, 2004.
[22] P. R. Villeneuve, S. Fan, S. G. Johnson, and J. D. Joannopoulos, "Three-dimensional photon confinement in photonic crystals of low-dimensional periodicity," *Proc. IEE Optoelectron.*, vol. 145, pp. 384–390, 1998.
[23] J. K. Hwang, H. Y. Ryu, D. S. Song, I. Y. Han, H. W. Song, H. K. Park, Y. H. Lee, and D. H. Jang, "Room-temperature triangular-lattice two-dimensional photonic bandgap lasers operating at 1.54 μm," *Appl. Phys. Lett.*, vol. 76, pp. 2982–2984, 2000.
[24] J. K. Hwang, H. Y. Ryu, D. S. Song, I. Y. Han, H. K. Park, D. H. Jang, and Y. H. Lee, "Continuous room-temperature operation of optically pumped two-dimensional photonic crystal lasers at 1.6 μm," *IEEE Photon. Technol. Lett.*, vol. 12, no. 10, pp. 1295–1297, Oct. 2000.
[25] T. Yoshie, O. B. Shchekin, H. Chen, D. G. Deppe, and A. Scherer, "Quantum dot photonic crystal lasers," *Electron. Lett.*, vol. 38, pp. 967–968, 2002.
[26] H. G. Park, S. K. Kim, S. H. Kwon, G. H. Kim, S. H. Kim, H. Y. Ryu, S. B. Kim, and Y. H. Lee, "Single-mode operation of two-dimensional photonic crystal laser with central post," *IEEE Photon. Technol. Lett.*, vol. 15, no. 10, pp. 1327–1329, Oct. 2003.
[27] M. Imada, S. Noda, A. Chutinan, T. Tokuda, M. Murata, and G. Sasaki, "Coherent two-dimensional lasing action in surface-emitting laser with triangular-lattice photonic crystal structure," *Appl. Phys. Lett.*, vol. 75, pp. 316–318, 1999.
[28] S. Noda, M. Yokoyama, M. Imada, A. Chutinan, and M. Mochizuki, "Polarization mode control of two-dimensional photonic crystal laser by unit cell structure design," *Science*, vol. 293, pp. 1123–1125, 2001.
[29] R. Colombelli, K. Srinivasan, M. Troccoli, O. Painter, C. F. Gmachl, D. M. Tennant, A. M. Sergent, D. L. Sivco, A. Y. Cho, and F. Capaso, "Quantum cascade surface-emitting photonic crystal laser," *Science*, vol. 302, pp. 1374–1377, 2003.
[30] K. Srinivasan, O. Painter, R. Colombelli, C. F. Gmachl, D. M. Tennant, A. M. Sergent, M. Troccoli, and F. Capaso, "Lasing mode pattern of quantum cascade photonic crystal surface-emitting microcavity laser," *Appl. Phys. Lett.*, vol. 84, pp. 4164–4166, 2004.
[31] J. Huh, J. K. Hwang, H. Y. Ryu, and Y. H. Lee, "Nondegenerate monopole mode of single defect two-dimensional triangular photonic bandgap cavity," *J. Appl. Phys.*, vol. 92, pp. 654–659, 2002.
[32] H.-G. Park, S.-H. Kim, S.-H. Kwon, Y.-G. Ju, J.-K. Yang, J.-H. Baek, S.-B. Kim, and Y.-H. Lee, "Electrically driven single-cell photonic crystal laser," *Science*, vol. 305, pp. 1444–1447, 2004.
[33] W. D. Zhou, J. Sabarinathan, P. Bhattacharya, B. Kochman, E. W. Berg, P. C. Yu, and S. W. Pang, "Characteristics of a photonic bandgap single defect microcavity electroluminescent device," *IEEE J. Quantum Electron.*, vol. 37, no. 9, pp. 1153–1160, Sep. 2001.
[34] J. Topol'ancik, S. Pradhan, P.-C. Yu, S. Ghosh, and P. Bhattacharya, "Electrically injected photonic crystal edge-emitting quantum-dot light source," *IEEE Photon. Technol. Lett.*, vol. 16, no. 4, pp. 960–962, Apr. 2004.
[35] T. D. Happ, M. Kamp, A. Forchel, J.-L. Genter, and L. Goldstein, "Two-dimensional photonic crystal coupled-defect laser diode," *Appl. Phys. Lett.*, vol. 82, pp. 4–6, 2003.
[36] M. Fujita, A. Sakai, and T. Baba, "Ultrasmall and ultralow threshold GaInAsP-InP microdisk injection lasers: design, fabrication, lasing characteristics, and spontaneous emission factor," *IEEE J. Sel. Topics Quantum Electron.*, vol. 5, no. 3, pp. 673–681, May-Jun. 1999.
[37] J. L. Jewell, J. P. Harbison, A. Scherer, Y. H. Lee, and L. T. Florez, "Vertical-cavity surface-emitting lasers: design, growth, fabrication, characterization," *IEEE J. Quantum Electron.*, vol. 27, no. 6, pp. 1332–1346, Jun. 1991.
[38] L. A. Coldren and S. W. Corzine, *Diode Lasers and Photonic Integrated Circuits*. New York: Wiley, 1995.
[39] C. W. Wilmsen, H. Temkin, and L. A. Coldren, *Vertical-Cavity Surface-Emitting Lasers: Design, Fabrication, Characterization, and Applications*. New York: Cambridge Univ. Press, 1999.
[40] K. Inoshita and T. Baba, "Fabrication of InGaAsP/InP photonic crystal lasers by ICP etching and control of resonant mode in point and line composite defects," *IEEE J. Sel. Topics Quantum Electron.*, vol. 9, no. 4, pp. 1347–1354, Jul.-Aug. 2003.
[41] J. Vuckovic, M. Loncar, H. Mabuchi, and A. Scherer, "Design of photonic crystal microcavities for cavity QED," *Phys. Rev. E*, vol. 65, p. 016608, 2001.
[42] H. C. Casey, Jr. and M. B. Panish, *Heterostructure Lasers, Part B: Materials and Operating Characteristics*. New York: Academic, 1978.
[43] M. Fujita, R. Ushigome, and T. Baba, "Large spontaneous emission factor of 0.1 in a microdisk injection laser," *IEEE Photon. Technol. Lett.*, vol. 13, no. 5, pp. 403–405, May 2001.
[44] R. E. Slusher, A. F. J. Levi, U. Mohideen, S. L. Mcall, S. J. Pearton, and R. A. Logan, "Threshold characteristics of semiconductor microdisk lasers," *Appl. Phys. Lett.*, vol. 63, pp. 1310–1312, 1993.
[45] J. Vuckovic, O. Painter, X. Yong, A. Yariv, and A. Scherer, "Finite-difference time-domain calculation of the spontaneous emission coupling factor in optical microcavities," *IEEE J. Quantum Electron.*, vol. 35, no. 8, pp. 1168–1175, Aug. 1999.
[46] D. Z. Garbuzov, V. V. Agaev, Z. N. Sokolova, V. B. Khalfin, and V. P. Chalyi, "Recombination processes in InGaAsP/InP double heterostructures emitting at $\lambda = 1 - 1.5\ \mu$," *Sov. Phys. Semicond.*, vol. 18, pp. 665–670, 1984.
[47] P.-T. Lee, J. R. Cao, S.-J. Choi, Z.-J. Wei, J. D. O'Brien, and P. Daniel Dapkus, "Operation of photonic crystal membrane lasers above room temperature," *Appl. Phys. Lett.*, vol. 81, pp. 3311–3313, 2002.
[48] G. Björk, A. Karlsson, and T. Yamamoto, "On the linewidth of microcavity lasers," *Appl. Phys. Lett.*, vol. 60, pp. 304–306, 1992.
[49] U. Mohideen, R. E. Slusher, F. Jahnke, and S. W. Koch, "Semiconductor microlaser linewidths," *Phys. Rev. Lett.*, vol. 73, pp. 1785–1788, 1994.
[50] H.-G. Park, Y.-G. Ju, S.-H. Kwon, S.-B. Kim, and Y.-H. Lee, "Characteristics of two-dimensional photonic crystal laser with central post," presented at the *PECS-V*, Kyoto, Japan, 2004.

Hong-Gyu Park was born in Seoul, Korea, in 1976. He received the B.S., M.S., and Ph.D. degrees from the Department of Physics, Korea Advanced Institute of Science and Technology (KAIST), Daejeon, in 1998, 2000, and 2004, respectively. During his Ph.D. work, he studied the design, fabrication, and characterization of photonic crystal light-emitting structures.

He is currently with the Department of Chemistry and Chemical Biology, Harvard University, Cambridge, MA.

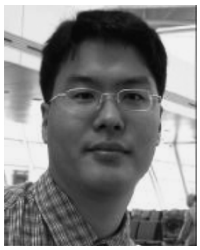

Se-Heon Kim was born in Seoul, Korea, in 1978. He received the B.S. and M.S. degrees from the Department of Physics, Korea Advanced Institute of Science and Technology (KAIST), Daejeon, Korea, in 2000 and 2002, respectively, where he is currently working toward the Ph.D. degree in photonic crystal devices.

Min-Kyo Seo was born in Seoul, Korea, in 1981. He received the B.S. and M.S. degrees from the Department of Physics, Korea Advanced Institute of Science and Technology (KAIST), Daejeon, in 2002 and 2004, respectively. He is currently working toward the Ph.D. degree at Department of Physics of KAIST.

His main interest lies on dynamics of semiconductors.

Young-Gu Ju received the B.S., M.S., and Ph.D. degrees from the Department of Physics, Korea Advanced Institute of Science and Technology, Daejeon, in 1992, 1994, and 1998, respectively. During his Ph.D. work, he studied the design, fabrication, and characterization of vertical-cavity surface-emitting laser (VCSEL).

He worked as a Visiting Engineer at University of California at Santa Barbara and developed coarse wavelength-division multiplexing VCSEL array. He continued his research at Electronics and Telecommunication Research Institute (ETRI), Daejeon. During his stay at ETRI, he worked on long-wavelength VCSELs. He is currently working at Department of Physics Education, KyungPook National University, Daegu, Korea.

Sung-Bock Kim was born in Daejeon, Korea, in 1965. He received the B.S., M.S., and Ph.D. degrees in physics from Yonsei University, Seoul, Korea, in 1990, 1992, and 2005, respectively.

In 1993, he joined the Electronics and Telecommunication Research Institute (ETRI), Daejeon, Korea, as a Member of Research Staff in the Basic Research Laboratory. With a research background in compound semiconductor epitaxy growth, he is currently studying the optoelectronic materials and photonics devices grown by MOCVD.

Yong-Hee Lee received the M.S. degree in applied physics from the Korea Advanced Institute of Science and Technology (KAIST), Daejon, and the Ph.D. degree in optical sciences from the University of Arizona, Tucson, in 1979 and 1986, respectively.

In 1987, he joined AT&T Bell Laboratories, Holmdel, NJ. There, he pioneered the first proton-implanted vertical-cavity surface-emitting laser (VCSEL) in 1990. He has continued his research on VCSELs after he joined the Department of Physics, KAIST, in 1991. Recently, his main interest lies in photonic crystal laser structures and photonic integrated optical circuits. He has coauthored more than 100 international journal papers related to VCSELs and photonic bandgap laser structures.

Dr. Lee received the National Academy of Sciences Award (Natural Science) in 2002 and the IEEE LEOS Distinguished Lecturer Award in 2003.